Intrinsic thermodynamic and kinetic properties of Sb electrodes for Li-ion and Na-ion batteries: Experiment and theory

ARTICLE *in* JOURNAL OF MATERIALS CHEMISTRY A · JUNE 2013

Impact Factor: 7.44 · DOI: 10.1039/C3TA11568B

Journal of Materials Chemistry A

RSC Publishing

PAPER

View Article Online
View Journal | View Issue

Cite this: J. Mater. Chem. A, 2013, 1, 7985

Intrinsic thermodynamic and kinetic properties of Sb electrodes for Li-ion and Na-ion batteries: experiment and theory

Loïc Baggetto,*[a] P. Ganesh,*[b] Che-Nan Sun,[a] Roberta A. Meisner,[ac] Thomas A. Zawodzinski[ad] and Gabriel M. Veith*[a]

A detailed comparative study between the electrochemical lithiation and sodiation of pure antimony (Sb), relating changes in structural, thermodynamic, kinetic and electrochemical properties has been carried out. For this purpose, a wide range of measurements using electrochemical (galvanostatic cycling, GITT, PITT), X-ray diffraction (XRD) and X-ray photoelectron spectroscopy (XPS) methods as well as density functional theory (DFT) based investigations have been undertaken. Assessment of the thermodynamics reveals that the reaction proceeds identically during the first and second cycles for Li whereas it differs between the first and subsequent cycles for Na as the reaction with Na proceeds through a different pathway associated with the formation of amorphous Na_xSb phases. For the first time we rationalize the amorphization of Na_xSb phases by the long ranged strain propagation due to Na-vacancy compared to Li–Sb. At full discharge, our XRD results show for the first time that a minor fraction of hexagonal Li_3Sb forms concomitantly with cubic Li_3Sb. The XRD results confirm that Sb crystallizes into hexagonal Na_3Sb at full sodiation. The kinetics of the reaction is assessed by rate performance tests which highlight that both Li and Na can diffuse rapidly throughout micron thick films at room temperature. However, it is found that the (de)insertion of Li provides lower overpotentials and larger storage capacities compared to Na. The difference in rate performance is complemented by diffusion coefficient determinations near the 0 V region where both materials are crystallized into M_3Sb (M = Li, Na). Interestingly, calculations show that the energy barrier for near-neighbor vacancy migration, predominant in these close-packed phases, is about twice for Na than for Li. Our analysis tries to relate the lower intrinsic diffusivity of Na compared to Li with the long-range strain propagation induced by the former, thereby leading to an intrinsic origin of differences in rates, mechanical properties and amorphization. Finally, the surface chemistry of Sb electrodes cycled in $NaClO_4$ dissolved in pure PC with(out) the addition of 5 wt% EC or FEC shows presence of ethers and NaF for the EC- and FEC-based electrolytes, respectively, and SEI films rich in Na-based carbonates.

Received 19th April 2013
Accepted 24th May 2013

DOI: 10.1039/c3ta11568b

www.rsc.org/MaterialsA

1 Introduction

The sodium-ion battery concept is attracting a lot of attention as an alternative energy storage system to lithium-ion technology.[1,2] The use of sodium is environmentally sustainable and cheaper thanks to the wide abundance of the element. Moreover, the electrochemical Na/Na^+ redox potential is only about 0.3 V above that of Li/Li^+, which renders the Na-ion battery concept an attractive energy storage alternative.[1,2] However, implementing this technology requires the development of suitable electrode materials.[1–5] Among the pure elements with suitable redox potentials *versus* Na/Na^+ (*e.g.* C, Ge, Sn, Sb, Pb) for consideration as anode materials, Sn ($Z = 50$) appears most promising from the perspectives of cost, high storage capacity (847 mA h g^{-1} corresponding to $Na_{15}Sn_4$) and low voltage operation (~0.2 to 0.3 V *vs.* Na/Na^+).[3] From the perspective of faster reaction kinetics, Sb ($Z = 51$) has shown to have an excellent potential for use as an anode material for Na-ion battery[4,5] while having a theoretical capacity of 660 mA h g^{-1} corresponding to the formation of Na_3Sb.[4–7]

The phase transformations occurring in bulk Sb during Na-ion (de)insertion have recently been reported by Darwiche *et al.* using *in situ* XRD,[4] and the reaction proceeds with the formation of an amorphous phase until cubic and hexagonal Na_3Sb polymorphs are formed. Intriguingly, the authors stated that Li is more kinetically limited than Na. This statement was partly

[a]Materials Science and Technology Division, Oak Ridge National Laboratory, 1 Bethel Valley Rd, Oak Ridge, TN 37831, USA. E-mail: baggettol@ornl.gov; veithgm@ornl.gov
[b]Center for Nanophase Materials Sciences, Oak Ridge National Laboratory, 1 Bethel Valley Rd, Oak Ridge, TN 37831, USA. E-mail: ganeshp@ornl.gov
[c]Department of Materials Science and Engineering, University of Tennessee Knoxville, Knoxville, TN 37996, USA
[d]Department of Chemical and Biomolecular Engineering, University of Tennessee Knoxville, Knoxville, TN 37996, USA

based on an erroneous theoretical capacity reported as 610 mA h g^{-1} (ref. 4) instead of 660 mA h g^{-1},[6,7] and the conclusion was supported by comparing the relative decrease of reversible capacity of Li–Sb and Na–Sb from C/2 to 4 C. However, the authors did not consider that a substantially higher storage capacity was measured for Li at C/2 (622 mA h g^{-1}, 94.2% of theoretical), which was fully maintained at 2 C, whereas the storage capacity for Na was found to be much lower (537 mA h g^{-1}, 81.3% of theoretical) at C/2, and 506 mA h g^{-1} at 2 C. Moreover, the definition of C-rate current given by the authors takes into account the amount of Na exchanged per hour such that the commonly accepted C-rate values based on the time spent per (dis)charge step are in fact 3 times lower. Thus, 4 C in their definition corresponds to only 4/3 C. Also, the fact that Li reversibly forms all the stable phases during discharge and reversibly goes directly from Li_3Sb to Sb during charge over multiple cycles,[8] while Na_3Sb only forms amorphous Na_xSb phases[4] emphasizes that Li may be diffusing faster than Na and not the other way around. Finally, the claim that Li is kinetically more limited than Na was not substantiated by rate capability experiments at high currents or by the determination of diffusion coefficients.

Beyond these electrochemical considerations, the authors attributed the better capacity retention of Na–Sb compared to Li–Sb to a decreased volume expansion upon going from Sb (181 Å) to hexagonal Na_3Sb (237 $Å^3$) compared to rock salt Li_3Sb (284 $Å^3$).[4] Unfortunately, the authors did not take into account that the volume of the hexagonal $P6_3/mmc$ structure includes only 2 formula units of Na_3Sb (PDF 03-065-3523) whereas the cubic $Fm\bar{3}m$ structure of Li_3Sb contains 4 formula units (PDF 03-065-3011). As a result, the volume per formula unit in $P6_3/mmc$ Na_3Sb is 118.5 $Å^3$ as opposed to only 71 $Å^3$ for $Fm\bar{3}m$ Li_3Sb – note that $P6_3/mmc$ Li_3Sb (PDF 03-065-3515) has a volume of about 80 $Å^3$ per formula unit. The volume of the $R\bar{3}m$ Sb structure reported above is measured for 6 Sb atoms, which corresponds to about 30 $Å^3$ per atom. Consequently, the volume expansion from Sb to Li_3Sb is about 135% (final volume to initial volume ratio of 2.35) but increases to about 293% for the alloying of Sb into Na_3Sb (final volume to initial volume ratio of 3.93). Obviously, the expected volume expansion resulting from the formation of Na_3Sb is much larger than for Li_3Sb and therefore cannot explain the better cycle life observed for Na. Instead we suspect that the repeated formation of only one crystalline phase for Na (Na_3Sb) against the repeated formation of three crystalline phases for Li (Sb, Li_2Sb and Li_3Sb) reduces the amount of anisotropic mechanical stress and is more likely responsible for the better cycling of Na with Sb. In addition, it may also be the case that the formation of a thinner or more stable SEI for the Na–Sb electrode leads to lower internal impedance, thereby improving capacity retention after prolonged cycling.

As a result, we have performed a comprehensive investigation comparing the reaction of Sb electrodes with Li and Na. Thin films are an ideal model system for studying the properties of binder-free and carbon-free electrodes and reveal intrinsic structure–property relationships.[9–11] The differences in reaction kinetics of micron-thick pure Sb sputter deposited films were measured by rate performance tests up to 10 C-rate. Moreover, we have characterized the quasi-equilibrium potential profiles during the first two cycles of the Li–Sb and Na–Sb systems using the Galvanostatic Intermittent Titration Technique (GITT). Interestingly, Hewitt *et al.* reported a marked increase in the discharge potential of Li–Sb during the second cycle,[8] as also observed in[4] and in our data. Our GITT measurements will demonstrate that this increase of potential is not thermodynamic in nature and is therefore related to an improvement of the reaction kinetics. Voltage predictions for both Li–Sb and Na–Sb systems were conducted using Density Functional Theory (DFT) calculations on the known crystallographic phases and compared to the galvanostatic and quasi-equilibrium data obtained with GITT. In addition, the apparent chemical diffusion coefficients of Li and Na determined using the potentiostatic intermittent titration technique (PITT) are provided, and qualitatively compared to first principle calculations of diffusion barriers in the M_3Sb structures.

Finally, we have investigated the Solid Electrolyte Interphase (SEI) formation in 1 M $NaClO_4$ in propylene carbonate (PC) electrolyte with(out) carbonate additives. The use of fluoroethylene carbonate (FEC) as an efficient additive to improve the capacity retention has been demonstrated for Na–Sb electrodes,[4,6] however, little understanding of its action mechanism has been reported. The differences in SEI chemistry measured by X-ray photoelectron spectroscopy (XPS) of Sb thin film electrodes in 1 M $NaClO_4$/PC electrolyte, with(out) FEC and ethylene carbonate (EC) additives will be discussed.

2 Experimental

2.1 Samples preparation

Sb films were prepared on roughened Cu foils using DC magnetron sputtering in a chamber with a base pressure typically below 10^{-6} Torr. A homemade Sb target (99.5%, Sigma-Aldrich) and Ar (99.99%, Air Liquide) were used as target material and sputtering gas at 20 mTorr deposition pressure and 20 W DC power. Film thickness was estimated using a quartz microbalance installed inside the chamber. After preparation, weighted discs were stored inside an Ar-filled glovebox. The thickness was back-calculated based on the weight of the samples and the expected density of Sb (6.7 g cm^{-3}).

2.2 Characterization

Electrochemical characterization was conducted at 25 °C inside a thermostated incubator using 2-electrode coin cells (2032 hardware, Hohsen) prepared inside an Ar-filled glovebox. The cells consisted of pure Na (Sigma-Aldrich) or Li (Alfa Aesar) as counter electrodes, glass fiber separators impregnated by 1 M $NaClO_4$ in anhydrous PC (Sigma-Aldrich) or 1.2 M $LiPF_6$ in dimethyl carbonate (DMC) and EC (Novolyte) electrolyte solutions, and Sb thin films as working electrodes. 5 wt% of anhydrous FEC or EC (Sigma-Aldrich) was added to the Na-electrolyte for XPS studies. Galvanostatic cycling was performed on a Maccor 4000 series for electrodes with a surface area of 1.27 cm^2. 1 C-rate current corresponds to the current required to

(dis)charge the electrodes in 1 h. GITT profiles were measured during the first and second cycles with current pulses of C/10 for 0.5 h duration followed by rest periods of 2 h. For the apparent chemical diffusion coefficient determination, PITT was employed on identical electrodes of 1 μm thickness. The electrodes were fully discharged at C/10 till the potential reached 0 V maintained until the current dropped below C/120. Subsequently, repeated potential steps of 10 mV with current cut-off values of C/120 were applied until the potential reached 0.7 V.

For *ex situ* characterizations, specimens were extracted from coin cells inside an Ar-filled glovebox. For XPS samples were rinsed with anhydrous DMC and for XRD specimens were simply pressed onto a fiber paper to remove the excess electrolyte. Panalytical Xpert diffractometers equipped with Cu K_α and Mo K_α radiations and X'Celerator detectors were used. The pristine film was measured with Cu K_α radiation whereas fully discharged electrodes sealed with Kapton tape (25 μm) onto a glass slide inside an Ar glovebox were measured with Mo K_α radiation. Samples were brought to the diffractometer inside Ar-filled heat-sealed pouch bags and opened at the last minute. Surface chemistry was probed using a PHI 3056 XPS spectrometer equipped with Al K_α and Mg K_α sources (1486.6 and 1253.6 eV) at a measurement pressure below 10^{-8} Torr. The use of Mg K_α is useful for preventing an important overlap of Sb3d5/2 with a Na Auger line. Rinsed samples were transferred from the glovebox to the XPS chamber under vacuum using an air-tight transfer device. High resolution scans were acquired at 350 W with 23.5 eV pass energy and 0.05 eV energy step. Survey scans were measured at 350 W with 93.9 eV pass energy and 0.3 eV energy step. The binding energies were shifted by setting the adventitious carbon signal to 284.8 eV to account for charging. The spectra were deconvoluted using Gaussian–Lorentzian functions and a Shirley-type background with corresponding assignments presented.

2.3 Computational methods

DFT-based relaxation studies were performed using the plane-wave code VASP[12–14] and a Perdew–Burke–Ernzerhof exchange-correlation function. Spin polarization, a 215 eV kinetic energy cutoff and converged *k*-point meshes were used for all the calculations. Structural lattice parameters were obtained from the ICSD database and only the internal atomic coordinates were relaxed to obtain the voltage profiles (since our calculations are at 0 K while experiments are at room temperature) using the following formula: $V(x) = [E(M_xSb) - E(M_{x+\Delta x}Sb)]/\Delta x + E(M)$, where E is the DFT total energy, M = (Na, Li), x = M/Sb and E(M) is the bulk ground state total energy of the metal M.[15] Our previous study on Na_xSn (ref. 3) suggests that structural relaxations do not influence the voltages significantly for this family of binary compounds. Single vacancy diffusion barrier calculations for the M-atom were performed in a 2 × 2 × 2 supercell of the cubic Li_3Sb and the hexagonal Na_3Sb phases using the climbing image nudged-elastic-band[16] method till forces converged down to 0.01 eV $Å^{-1}$. A 6 × 6 × 8 and 4 × 4 × 4 *k*-point meshes were used for Na_3Sb and Li_3Sb supercells. All atoms were relaxed keeping the lattice parameter fixed allowing local strain relaxation around the vacancy at each point along the low energy barrier path. Only the nearest neighbor vacancy migration barrier was estimated because it dominates ion diffusion in close-packed phases.

3 Results and discussion

3.1 Comparison of the electrochemical responses during the reactions with Li and Na

The potential profiles of Sb thin film electrodes obtained during the first two cycles are presented in Fig. 1. Reversible capacities of 663 and 656 mA h g^{-1} are measured with Li (Fig. 1a), very close to the theoretical value (660 mA h g^{-1}). During Li-ion reaction the first discharge profile at C/10 is characterized by two successive plateaus at 0.82 and 0.78 V which correspond to the formation of Li_2Sb and Li_3Sb,[8] whereas the first charge profile displays a single plateau near 1.02 V that corresponds to the direct conversion of Li_3Sb into Sb.[8] As also observed in ref. 4 and 8 the first plateau of the second discharge is now shifted to 0.89 V whereas the second plateau remains at 0.78 V (inset). Given that the first plateau corresponds for both cycles to an amount of charge close to 2 Li/Sb, it is likely that the reaction from Sb to Li_2Sb is preserved, as confirmed by the *in situ* XRD results of Hewitt *et al.*[8] The difference in potential is thereby likely related to an improvement of the reaction kinetics of Sb. It is known that electrochemical cycling can cause a decrease in particle size (also referred to as electrochemically-driven grinding).[17,18] In turn, the formation of a material with a larger surface area and smaller particle size may be expected, both contributing to smaller overpotentials for the reaction. Here, the decrease in particle size is suggested by the broader line width and lower intensity of the XRD peaks attributed to Sb in Fig. 11 of ref. 8. Further support for the role of kinetics and not of thermodynamics is given by the GITT measurements. Indeed it is clear that no changes in quasi-equilibrium potentials are measured for Li–Sb during the first two discharges (Fig. 1b). In addition, as observed during the galvanostatic measurements at C/10, no differences are noticed between both charges. Looking in detail at the GITT measurements, we observe that the difference of potential between charge and discharge is now reduced from 0.2 V at C/10 to about 0.06 V, and could be further reduced if longer rest periods would be applied. This important decrease indicates that most of the potential difference measured during a galvanostatic measurement is related to the reaction kinetics and not to thermodynamic hysteresis.

In the case of the Na-ion reaction (Fig. 1c), the discharge at C/10 is composed of a plateau around 0.57 V followed by a somewhat more sloping plateau around 0.46 V, also observed in the dQ/dV plots in ref. 4. These features correspond to the formation of an amorphous phase, followed by the formation of cubic and hexagonal Na_3Sb phases, and ultimately leading to the presence of hexagonal Na_3Sb only.[4] During charge a pronounced plateau is visible near 0.78 V followed by a sloping plateau at about 0.86 V. The second discharge presents sloping plateaus around 0.72 and 0.5 V. Overall, reversible capacities of 542 and 525 mA h g^{-1} are measured during the first two cycles, which represent about 80% of the theoretical value. The lower than expected value was also measured on bulk powder

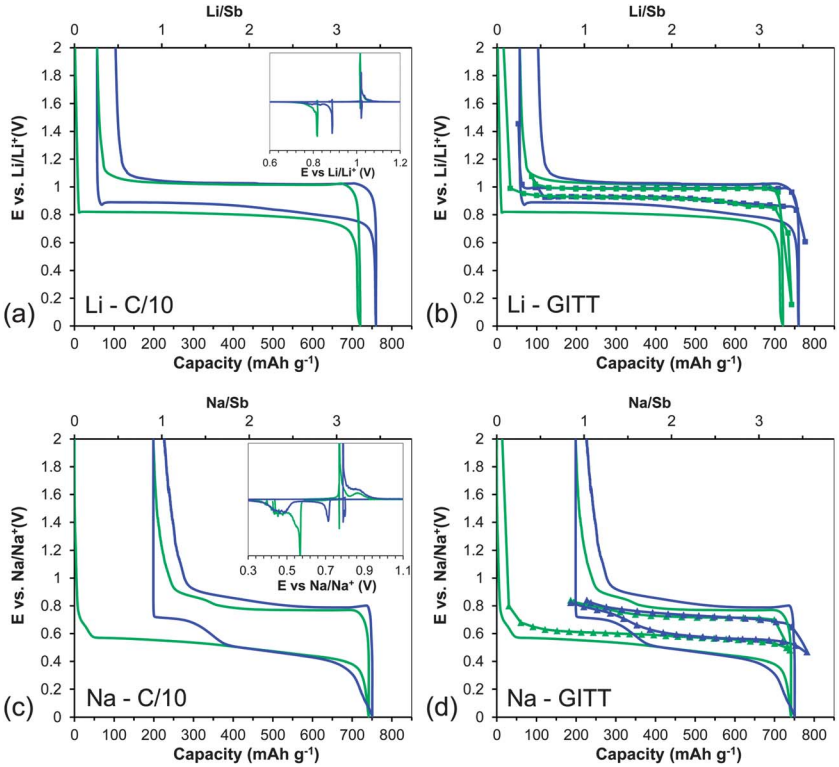

Fig. 1 Electrochemical potential profiles during (a)–(c) constant current and (b)–(d) quasi-equilibrium (GITT) measurements obtained on Sb thin films electrodes, during the first (green) and second (blue) cycles, for the reaction with Li and Na. The inset shows the corresponding derivative plots. Cycling was performed at C/10 between 0 and 2 V. GITT was obtained with 0.5 h C/10 pulses separated by 2 h rest periods.

electrode[4] and is likely related to the absence of full desodiation. During quasi-equilibrium (Fig. 1d), the difference of potential between discharge and charge decreases by about half from about 0.3 V at C/10 to 0.15 V during GITT. The larger difference compared to Li can be due to the slower relaxation of the reaction kinetics but also to hysteresis due to the formation of an intermediate amorphous phase.[4] Both effects suggest that Na solid-state diffusion may be slower than for Li.

The voltage profiles predicted by DFT calculation have been obtained on both Li– and Na–Sb systems (Fig. 2). For Li (Fig. 2a and b), the calculation takes into account the formation of hexagonal Li_2Sb ($P\bar{6}2c$) and of the cubic and hexagonal Li_3Sb polymorphs (cubic $Fm\bar{3}m$ and hexagonal $P6_3/mmc$) of which only the high pressure cubic $Fm\bar{3}m$ phase has been reported to form electrochemically.[8] For Na (Fig. 2c and d), the calculation was based on the formation of monoclinic NaSb ($P2_1/c$) and hexagonal Na_3Sb ($P6_3/mmc$). In both cases, a fairly good agreement is found between the predicted voltages and the experimental values. In the case of Li, the predicted voltages of the cubic and hexagonal Li_3Sb phases are extremely close, respectively at 0.818 and 0.813 V, suggesting the possible coexistence of these phases as seen in our experimental XRD measurements (see section 3.2).

3.2 Differences in crystal structure at full lithiation and sodiation

The changes in crystal structure for fully discharged cells were studied by XRD (Fig. 3). In the case of Li the fully lithiated Sb electrode is mainly composed of cubic $Fm\bar{3}m$ Li_3Sb although there is clear indication that hexagonal $P6_3/mmc$ Li_3Sb also forms, as evidenced by the presence of some of the strongest peaks expected for the phase, especially near $2\theta = 24.5°$. Based on Rietveld refinements, the hexagonal phase represents a minor proportion around 4 wt%. This result complements the *in situ* XRD results of Hewitt *et al.*,[8] and likely results from the use of a thick layer (starting thickness of 4 μm and estimated thickness at full lithiation around 9.5 μm) measured using Mo K_α radiation. It could also be that the presence of the hexagonal phase results from the conversion of the cubic phase if a sufficiently long rest is given, as here during *ex situ* measurements. As discussed earlier, the coexistence of these phases is thermodynamically possible, as indicated by the very close predicted voltages of 0.818 and 0.813 V for the cubic and hexagonal phases, respectively. The refined lattice parameters for the cubic Li_3Sb phase are $a = b = c = 6.5768$ Å (±0.0004), in good agreement with the former work.[8] In the case of Na the fully sodiated electrode is composed of hexagonal $P6_3/mmc$ Na_3Sb, in good agreement with the results of Darwiche *et al.*[4] The refined lattice parameters for the hexagonal Na_3Sb phase are $a = b = 5.3397$ Å (±0.0006) and $c = 9.4915$ Å (±0.0013), in good agreement with the ICSD data (PDF 01-074-1162). These results confirm the difference in structure of the electrochemical end-members Li_3Sb and Na_3Sb polymorphs where Li prefers to alloy into the high pressure cubic phase whereas Na prefers to alloy in the ambient hexagonal phase.

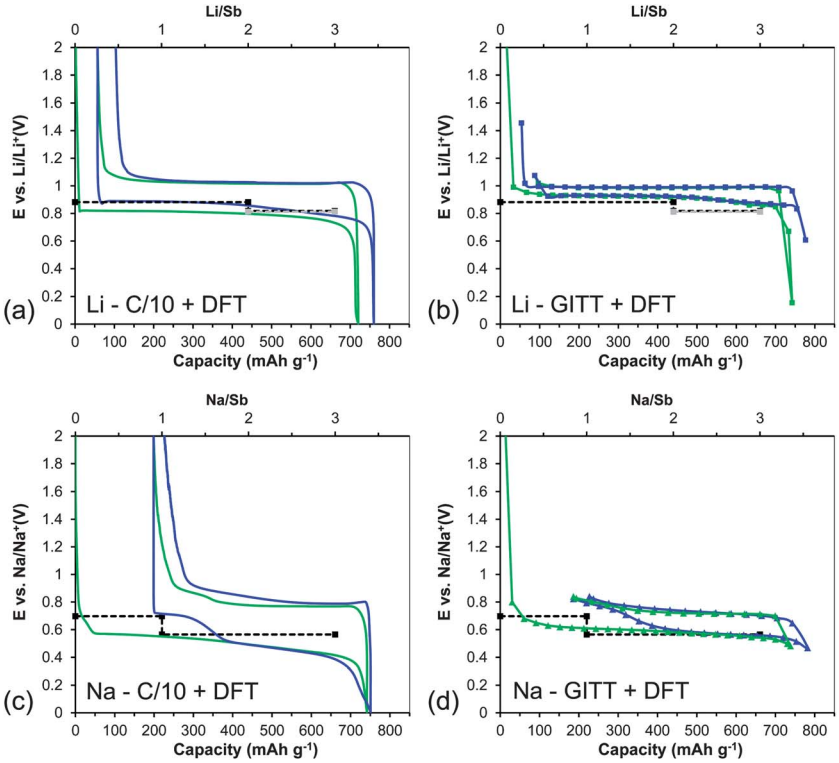

Fig. 2 Comparison of the potential profiles for Sb electrodes during the reaction with Li and Na predicted from DFT calculations (black dashed lines) with the (a)–(c) electrochemical constant current and (b)–(d) quasi-equilibrium (GITT) potential profiles presented in Fig. 1. First and second cycles are represented by green and blue curves, respectively. For Li, the DFT predicted potentials for the formation of cubic $Fm\bar{3}m$ Li_3Sb (black) and hexagonal $P6_3/mmc$ Li_3Sb (gray) are both given, resulting in plateaus at 0.818 and 0.813 V, respectively.

3.3 Comparison of the reaction kinetics with Li and Na

The rate performance of Sb thin films for currents from C/10 to 10 C was measured on several thick electrodes for various cycles and is presented for the first cycle (Fig. 4). First, the rate performance was investigated on thick electrodes of similar thicknesses during discharge at 10 C with charge currents of C/10. The increases in overpotential measured during discharge at 10 C are similar for Li and Na at about 0.2 V (Fig. 4a and b). However, the total amount of charge inserted into Sb is higher with Li, as shown by the discharge capacities obtained at 10 C for Li and Na, 640 *vs.* 600 mA h g^{-1} respectively, and also by the reversible capacities recovered during charge at C/10 for Li and Na, 580 *vs.* 450 mA h g^{-1} respectively. The rate performance was also measured during charge with currents up to 10 C after a slow discharge at C/10 (Fig. 4c and d). In the case of Li, the shape of the charge profiles is the same and the profile at 10 C is simply shifted upwards by about 0.2 V. Moreover, the amounts of Li recovered from the electrode are very close (625 *vs.* 663 mA h g^{-1} for 10 and 0.1 C at 2 V, respectively), which indicates excellent kinetics of Li-ion removal. In the case of Na, the profiles are somewhat different. At 5 C the profile shape is more or less retained but a large potential increase followed by a decrease is visible at the start of the charge, and is further pronounced at 10 C. These features are generally indicative of impeding nucleation/growth processes due to limited diffusion or impeding nuclei surface energetics, and suggests that the nucleation of the Na_xSb amorphous clusters from Na_3Sb is energetically more demanding at high rates. The position of the 'plateau' shifts from about 0.8 V to around 1.0 and 1.65 V for 5 and 10 C, respectively. Moreover, the amount of recovered Na at 2 V importantly decreases from 542 mA h g^{-1} at C/10 to only 418 and 347 mA h g^{-1} at 5 and 10 C, respectively.

Extending the charge cut-off potential up to 2.5 V helps to recover more capacity but at the price of cell voltage. Although the thicknesses of the electrode used for Na (1.4 and 1.6 μm at 5 and 10 C) are larger than that used for Li (1.2 μm at 10 C), the much higher increase in overpotentials for Na is indicative that the reaction of Sb with Na is kinetically more limited than with Li, as discussed next for electrodes with quasi-identical thicknesses.

Further evidence of the slower reaction rate of Na–Sb compared to Li–Sb are presented in Fig. 5 for cells that were discharged at 10 C followed by a deep discharge at C/10, and charged at 10 C followed by a deep charge at C/10. In this experiment, the thickness of the starting Sb electrode used with Li (Fig. 5a) is slightly thicker than that used for Na (Fig. 5b), *i.e.* 1.3 *vs.* 1.2 μm, respectively. The position of the plateau during charge at 10 C is similar for Li around 1.2 V in both Fig. 4 and 5, however, the plateau for Na is now around 1.45 V against 1.65 V presented previously (Fig. 4). This difference results in the use of a thinner film (1.2 instead of 1.6 μm). Nonetheless, it is clear that the increase in overpotential is much lower for Li (~0.2 V) compared to Na (~0.65 V). Moreover, comparing the relative contribution of the capacities spent during the 10 C discharge

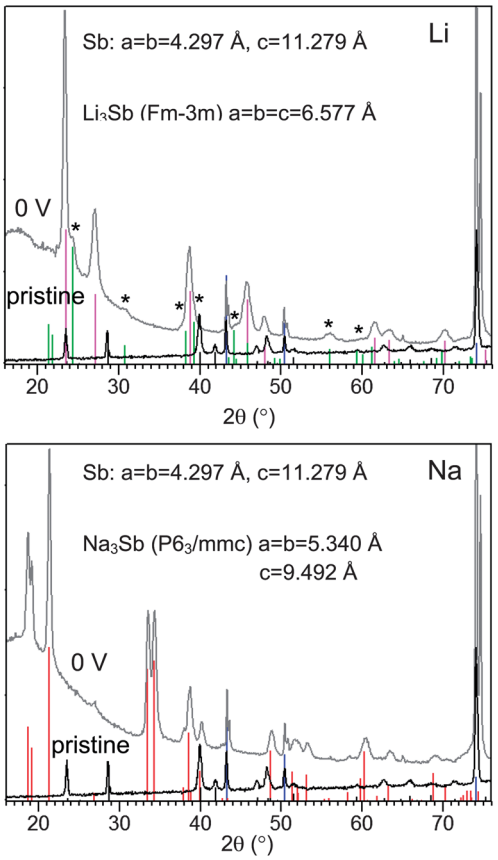

Fig. 3 XRD patterns collected for fully discharged (0 V) Sb electrodes during Li and Na reactions. The blue, red, fushia and green vertical bars represent the diffraction lines expected for Cu foil and the Na_3Sb ($P6_3/mmc$), Li_3Sb ($Fm\bar{3}m$) and Li_3Sb ($P6_3/mmc$) structures, respectively. (*) represent the diffraction lines observed for hexagonal Li_3Sb. The pattern for Sb was acquired using Cu K_α radiation and patterns of discharged electrodes covered with Kapton tape were measured with Mo K_α radiation. For convenience, 2θ values are reported for Cu K_α radiation.

and C/10 deep discharge steps, it is clear that more Li can be inserted into Sb during the discharge step at 10 C. Similarly, more Li can be extracted from Sb during the high current charge. Quantitatively, it can be calculated that the ratios of the capacities spent during the 10 C current steps to the total capacity are equal to 0.88 and 0.93 for Li during discharge and charge, respectively, whereas the ratios are equal to 0.74 and 0.71 for Na, during discharge and charge respectively. The much lower values obtained for Na further confirm that Na is more kinetically limited than Li.

Darwiche *et al.* stated that Li is more kinetically limited than Na during the removal of the alkali ion.[4] The authors based their conclusion on the higher relative decrease of reversible capacity from C/2 to 4 C which they measured, while using a different definition of the C-rate current than that related to the time of the reaction which we use. Moreover, they did not take into account that a substantially higher storage capacity was measured for Li at C/2 (622 mA h g^{-1}, 94.2% of theoretical) and was fully maintained at 2 C, whereas the storage capacity for Na was found to be much lower (537 mA h g^{-1}, 81.3% of theoretical) at C/2, and 506 mA h g^{-1} at 2 C compared to 660 mA h g^{-1} theoretical. Assuming that the full reaction is achieved during discharge up to the composition Na_3Sb, as suggested by the XRD results (*cf.* Fig. 3 and ref. 4), the lower initial reversible capacity reported for Na (537 against 622 mA h g^{-1})[4] is indicative that some Na is trapped inside the electrode and cannot be fully removed. Based on the first cycle potential profile (Fig. 1c), one can calculate that the amount of trapped Na is about 0.5 Na/Sb. Although the mechanical degradation of the electrode due to the large volume expansion/contraction may cause a loss of electronic contact or the physical detachment of part of the active material, poorer kinetics suggested by our results, and the formation of an amorphous phase are possibly responsible for the lower storage capacities of Sb with Na compared to Li. Nonetheless, we should emphasize that the rates of Na-ion reaction are quite high, as found earlier for Cu_2Sb,[5] and given the large reversible capacity above 500 mA h g^{-1}, the results strengthen the good potential of Sb-based anodes for practical Na-ion battery applications.

In order to evaluate the differences in diffusion between Na and Li, we measured the apparent chemical diffusion coefficients during Li-ion and Na-ion removal from 0 V when both materials are crystallized into M_3Sb (M = Li, Na) compounds. We selected this region as the electrodes present a very similar composition but a different structure (cubic $Fm\bar{3}m$ Li_3Sb and hexagonal $P6_3/mmc$ Na_3Sb). Moreover, in order to apply the determination method based on PITT proposed by Wen *et al.*,[19] the reaction should take place in a solid solution region in principle achieved in steep regions of potential. The method relies on the determination of the apparent chemical diffusion coefficient using the relation

$$I(t) = \frac{Q\tilde{D}^{1/2}}{L\pi^{1/2}}\frac{1}{\sqrt{t}}$$

where $I(t)$ is the time-dependent electrical current during the titration process, Q is the total charge being titrated corresponding to the voltage step, L is the electrode thickness and $\tilde{D}$ the apparent chemical diffusion coefficient.

The corresponding diffusion coefficients along with a typical I *vs.* $t^{-0.5}$ plot are presented during PITT charge from 0 V in Fig. 6. For the calculation of the coefficients, the expected thicknesses were calculated based on the theoretical expansion derived from the crystallographic phases assuming uniaxial expansion of the 1 μm starting film perpendicular to the surface. The calculations thereby take into account that Na has to diffuse through thicker films, with thicknesses expected to be 2.35 and 3.93 μm for Li and Na, respectively. The use of starting films of the same thickness creates M_3Sb (M = Li, Na) films with different thicknesses, thus influencing the measurements of the rate performance and diffusion coefficients. However, from an application point of view, it is fairer to compare electrode which have similar storage capacities by using films with identical starting thicknesses. Overall, in that region of potential which is equivalent to a very narrow x composition change of $M_{3-x}Sb$ with $x \ll 0.1$, we find that the diffusion coefficient of Na is about 3–4 times higher at potentials lower than 0.35 V but starts to decrease substantially at larger potentials with the coefficient of Li being more than one order of magnitude larger at 0.7 V. The region above 0.35 V, especially near 0.7 V, is of

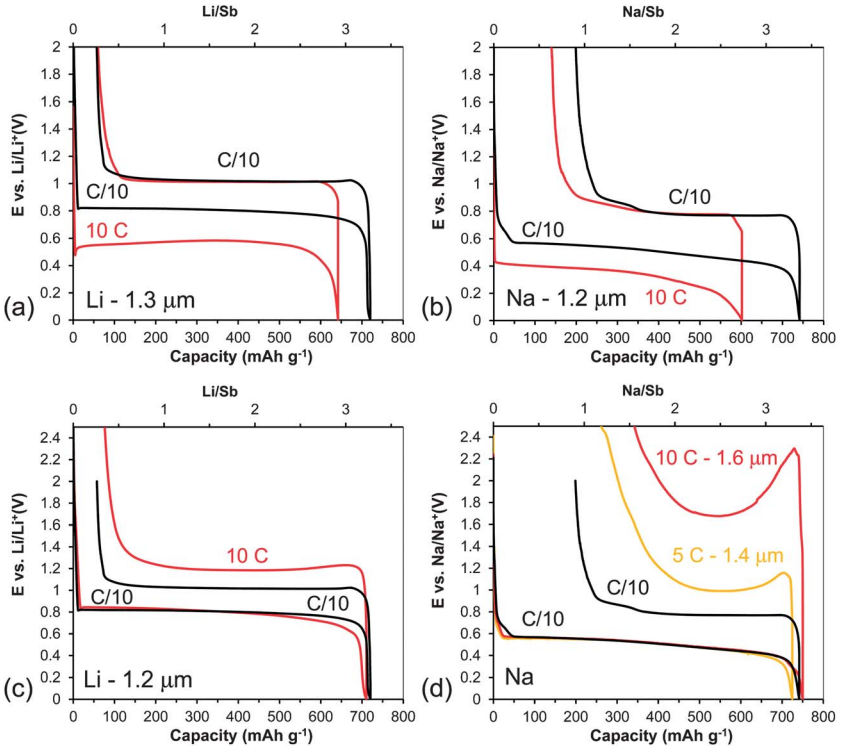

Fig. 4 Rate performance of Sb thin film electrodes during Li-ion and Na-ion insertion (discharge, (a) and (b)) and removal (charge, (c) and (d)) at currents from C/10 to 10 C-rate. (a and b) Following the discharges at 10 C, charges at C/10 were performed. (c and d) Prior to charges at 5 or 10 C, discharges at C/10 were performed. The profiles obtained at C/10 (black curves, Fig. 1) are inserted for reference.

particular significance as it corresponds to the start of the desodiation of Na_3Sb into amorphous Na_xSb which is accompanied with a large potential increase/decrease feature described previously (Fig. 4d). This important decrease in Na diffusion coefficient suggests that the impeding nucleation/growth may be diffusion controlled.

The discharge profiles obtained for Li and Na are both shifted by the same value of 0.2 V at 10 C (Fig. 4), which indicates that adding Na in the material is not much more impeding than adding Li. However, it is clear that the profile drops more quickly to 0 V in the case of Na, leading to a lower discharge capacity than with Li. The primary particle sizes estimated from the XRD patterns (Fig. 3) using Scherrer's equation[20] is similar for both films at around 15–20 nm. Thus, the lower capacity with Na may be related to a higher diffusion impedance induced by the larger thickness of the Na–Sb film compared to the Li–Sb film. During charge (ion removal), however, the increase in overpotential is larger and the recovered capacity is smaller for Na. The strong feature visible at the start of the charge (Fig. 4 and 5) in the case of Na, generally related to nuclei surface energy considerations or diffusion-limited growth, may be responsible for the apparent slower kinetics of Na suggested by the lower diffusion coefficient obtained at 0.7 V before.

3.4 Li and Na diffusivity predictions and associated strain relaxations

To see if the apparent slower reaction rate of Na was an intrinsic effect of Na_3Sb phase or due to the formation of amorphous phases in the experiments, nudged-elastic-band calculations[16] were performed in conjunction with DFT to obtain the nearest neighbor vacancy jump-migration barrier in a supercell. Fig. 7a and b show the vacancy migration path and the associated local atomic distortion around it. As seen in Fig. 8a, the vacancy migration barrier (E_m) can be as low as $E_m = 0.11$ eV/vacancy in cubic Li_3Sb (vacancy migrates from an octahedral site to a tetrahedral site), but is nearly two times higher in hexagonal Na_3Sb (vacancy migrates between two identical sites) with $E_m = 0.21$ eV/vacancy. Not only is the barrier low, but also the nearest neighbor jump distance is 2.82 Å in Li_3Sb as opposed to a slightly larger jump distance of 3.17 Å in Na_3Sb. Together, using the simple diffusion equation $D = D_0\exp(-\beta E_a)$, one can calculate that the diffusion coefficient is at least one order of magnitude lower in Na_3Sb than in cubic Li_3Sb. These prediction results suggest that a large portion of the measured differences in diffusivity between the two compounds is intrinsic. We also notice that the local strain field measured as the local atomic displacement from its ideal lattice position is more long-ranged in hexagonal Na_3Sb than in face-centered cubic Li_3Sb, as seen from Fig. 8b. In both cases the atomic local displacements relax to zero or negligibly small values with distance suggesting that our migration barrier calculations are converged with respect to the supercell size.

The long-ranged local strain propagation with Na might explain its ease of amorphization compared to Li in Sb. This also suggests a direct correlation between the local strain relaxation around a vacancy defect, vacancy migration barrier (and hence the diffusion barrier) and the long-range local strain

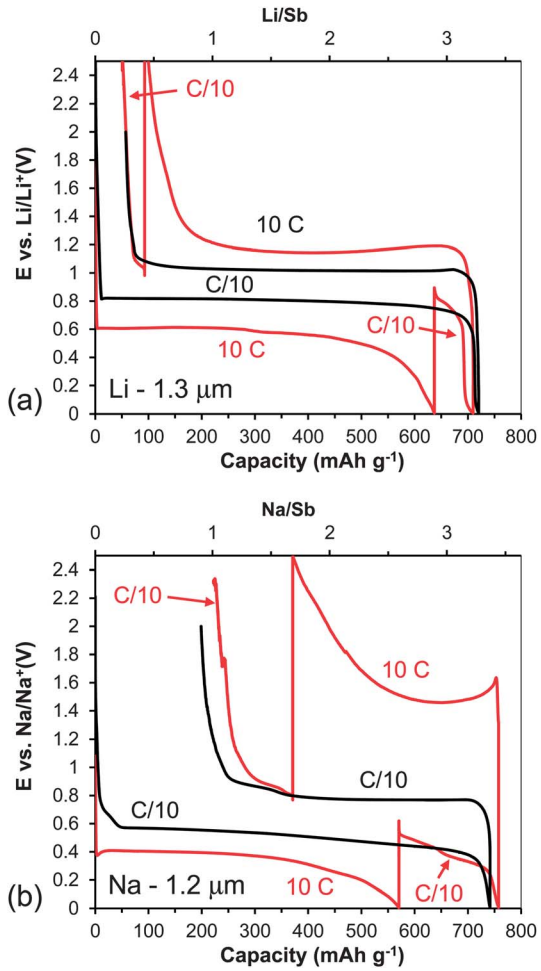

Fig. 5 Rate performance of Sb thin film electrodes during both insertion and removal of (a) Li and (b) Na using deep discharge at 10 C – C/10 and deep charge at 10 C – C/10.

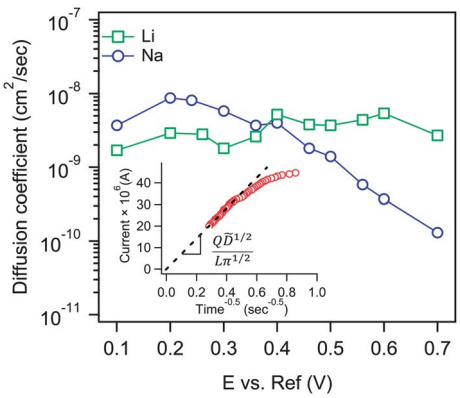

Fig. 6 Apparent chemical diffusion coefficient determination for Li^+ and Na^+ in M_3Sb (M = Li, Na) electrodes measured for 1.0 μm thick starting Sb electrodes. The region of interest is from 0 V upwards corresponding to the ion removal and a composition $M_{3-x}Sb$ with $x \ll 0.1$.

propagation away from the defect. Since the local strain relaxation and local strain propagation are related to the elastic constants, mainly the compressibility of the bulk materials, this

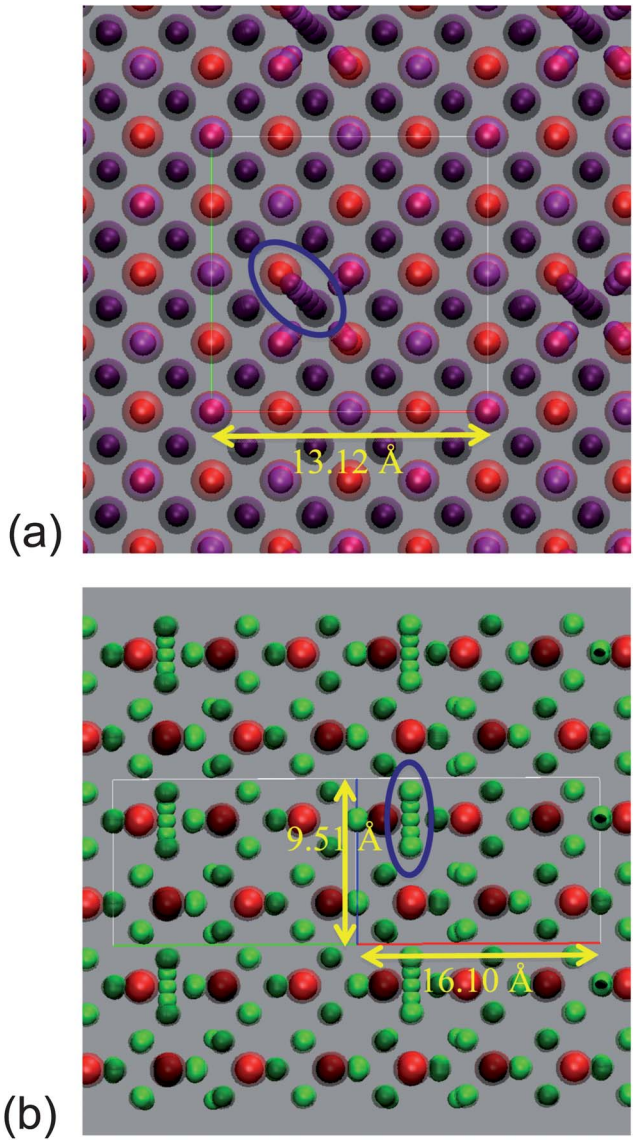

Fig. 7 Overlapping snapshots of cubic Li_3Sb and hexagonal Na_3Sb are shown along the lowest near-neighbor Na/Li-atom vacancy migration barrier pathway (shown inside oval outline) in (a) and (b) respectively. Ideal crystallographic lattice sites are shown as a black dotted outline. (Atom symbol: Sb (red), Li (magenta), Na (green).)

difference in diffusivity may thus be related to the differences in compressibilities of the two systems. Further investigation is required to establish this relationship over a wider class of close-packed intermetallics.

3.5 The effects of EC and FEC additives on the surface chemistry of fully (de)sodiated Sb electrodes

The surface chemistry obtained by XPS of Sb electrodes cycled in Na electrolytes without additive, and with EC or FEC additives along with the data for the pristine film is presented in Fig. 9. The pristine electrode is characterized by a metallic surface covered with multivalent oxides, as discussed earlier in detail for Cu_2Sb with the aid of Sb4d core level.[5] The similar features in the spectra of the cycled electrodes are discussed next. Generally, the discharged electrodes show a thicker SEI than the charged

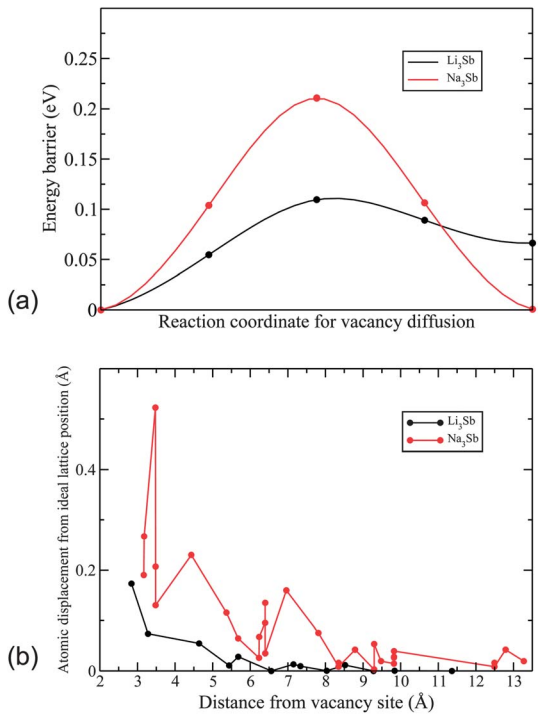

Fig. 8 Lowest near-neighbor Na/Li-atom vacancy migration energy barrier and local displacement of atoms from their ideal lattice site. (a) shows the migration barrier computed using climbing image nudged elastic band method. (b) presents the local displacement of atoms from their ideal lattice site (*i.e.* a measure of local strain) as we move away from the vacancy site. Na_3Sb shows large local atomic relaxation and as such a more long ranged strain propagation away from the vacancy site than Li_3Sb.

electrodes, as clearly observed by the lower F1s signal for the discharged electrode cycled in FEC, the higher signals for carbonates in C1s for discharged electrodes, as well as the presence of the signals of Sb for charged electrodes. The thinning of the SEI at full charge is attributed to the partial removal of the SEI due to oxidation of the surface film or due to mechanical detachment concomitant to electrode contraction associated with Na-ion removal also observed on Cu_2Sb[5] and Sn.[3] All cycled electrodes show the large presence of carbonates, especially at 0 V, evidenced by the binding energy around 289–289.5 eV in C1s matching the data obtained on a reference Na_2CO_3 powder.[3] The binding energies for Na are around 1072 eV for Na1s, 63 eV for Na2s and 30 eV for Na2p, very similarly to what was obtained earlier for the other Na anode systems.[3,5] For charged electrodes, the signals for Sb become visible for all electrolyte chemistries and the corresponding 3d and 4d binding energies for Sb are related to reduced $Sb^{\delta-}$ species, as found for Cu_2Sb,[5] which is likely indicative of Na–Sb bonds. The differences in surface chemistry for the different cycled electrodes are now discussed. In the case of EC additive, the presence of ethers functionalities, perhaps polyethylene oxide (PEO) generally found for EC-based Li electrolytes,[21] are clearly suggested by the signal around 286.5 eV in C1s whereas the other electrodes do not show the presence of ethers. For the electrodes cycled with FEC additive, the presence of NaF is suggested by the F1s spectra at an energy around 684.5 eV.[22] We suspect that the presence of NaF favors the good cycle life generally observed for Sb-based electrodes in $NaClO_4$ in PC/FEC electrolyte[4] and in $NaPF_6$ in EC/DEC/FEC electrolyte.[6]

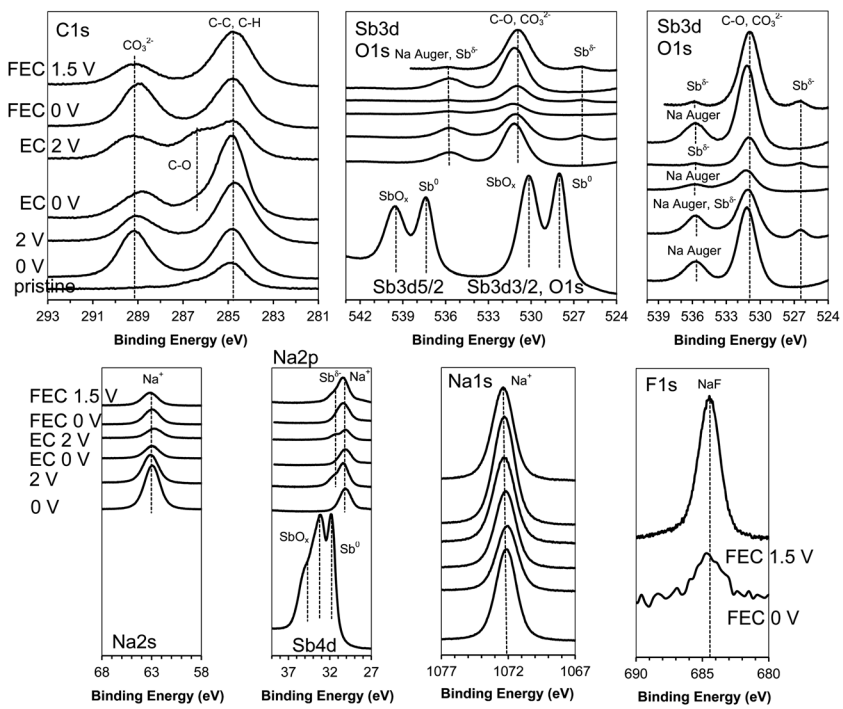

Fig. 9 C1s, O1s, Sb3d, Na2s, Na2p, Sb4d, Na1s and F1s XPS high resolution spectra for fully discharged and charged Sb thin film electrodes without additive and with EC or FEC additives. From bottom to top: pristine, discharged 0 V in PC, charged 2 V in PC, discharged 0 V in PC/EC, charged 2 V in PC/EC, discharged 0 V in PC/FEC and charged 1.5 V in PC/FEC. For simplicity, PC is omitted from the figure captions. The upper right figure does not show the spectra of the pristine material in order to enlarge the regions of interest. The F1s spectrum for FEC 0 V is from the survey scan. The Sb3d-O1s regions for the charged electrodes in EC- and FEC-based electrolytes were acquired with Mg K_α radiation to suppress an overlap with a Na Auger line.

4 Conclusions

The reaction thermodynamics and kinetics of pure Sb have been assessed using GITT and galvanostatic cycling at various currents from 0.1 to 10 C-rate on micron thick films. GITT results indicate that the reaction of Sb with Na yields larger hysteresis and/or non-relaxed overpotentials than the reaction with Li, which is likely due to the formation of amorphous phases in the case of Na. Moreover, in the case of Li, the GITT measurements demonstrate that the difference in potential profile during discharge between the first and subsequent cycles is related to the change in particle size improving the reaction kinetics and not to the reaction thermodynamics. The voltage profiles are in good agreement with voltage profiles predicted from DFT calculations. The structure of the fully discharged electrode revealed by XRD confirm that hexagonal Na_3Sb forms at full sodiation but reveal that cubic Li_3Sb as well as hexagonal Li_3Sb coexist at full lithiation, with the former being dominantly formed. The coexistence of both polymorphs is consistent with their very similar DFT predicted voltages. Regarding the reaction kinetics, both Li and Na show good performance with Sb electrodes easily discharged and charged at 10 C with high to moderate capacity retention for Li and Na, respectively. Nonetheless, it is clear that the reaction during charge (ion removal) is faster with Li, as indicated by the development of less overpotentials during the alkali ion removal. The higher kinetics of Li is further illustrated with the determination of diffusion coefficients using PITT during charge from 0 V, where Sb forms polymorph M_3Sb phases for both Li and Na. In that region of composition/potential, Li apparent diffusion coefficients are found to be 3–4 times lower at low voltages, and more than one order of magnitude higher than those of Na at 0.7 V. This is qualitatively consistent with a factor of two drop in the nearest neighbor ion-migration energy barrier and a shorter jump distance for Li in cubic Li_3Sb compared to Na in hexagonal Na_3Sb. The drop is possibly related to the long range effect of strain propagation in the hexagonal crystal lattice. We also essentially conclude that higher local strain relaxation effects lead to both slower diffusion and long-range strain propagation, with the latter favoring the formation of amorphous phases in the Na–Sb system. Conversely, smaller local strain relaxation leads to faster diffusion of Li in Li–Sb and more short-range elastic strain coupling. This analogy is similar to the concept of chemical expansivity,[23] but is now shown in intermetallics and is also shown to be related to the ease of amorphization of the solid in the presence of defects. The difference in strain relaxation results in avoiding the formation of amorphous phases in the Li–Sb system. The surface chemistry of electrodes cycled in 1 M $NaClO_4$ in PC electrolyte, and with EC and FEC additives is discussed. All electrodes generally present a thicker SEI rich in carbonates at full sodiation (discharge) whereas the fully desodiated (charged) electrodes clearly reveal the presence of reduced Sb species. In the case of EC additive, the presence of ethers is suggested whereas for FEC additive the presence of NaF is evidenced.

Acknowledgements

This work was supported by the U.S. Department of Energy (DOE), Basic Energy Sciences (BES), Materials Sciences and Engineering Division. Computations performed at the Center for Nanophase Materials Sciences (CNMS) are sponsored by DOE-BES.

References

1 V. Palomares, P. Serras, I. Villaluenga, K. B. Hueso, J. Carretero-González and T. Rojo, *Energy Environ. Sci.*, 2012, **5**, 5884–5901.
2 B. L. Ellis and L. F. Nazar, *Curr. Opin. Solid State Mater. Sci.*, 2012, **16**, 168–177.
3 L. Baggetto, P. Ganesh, R. P. Meisner, R. R. Unocic, J.-C. Jumas, C. A. Bridges and G. M. Veith, *J. Power Sources*, 2013, **234**, 48–59.
4 A. Darwiche, C. Marino, M. T. Sougrati, B. Fraisse, L. Stievano and L. Monconduit, *J. Am. Chem. Soc.*, 2012, **134**, 20805–20811.
5 L. Baggetto, E. Allcorn, A. Manthiram and G. M. Veith, *Electrochem. Commun.*, 2013, **27**, 168–171.
6 J. Qian, Y. Chen, L. Wu, Y. Cao, X. Ai and H. Yang, *Chem. Commun.*, 2012, **48**, 7070–7072.
7 L. Xiao, Y. Cao, J. Xao, L. Kovarik, Z. Nie and J. Liu, *Chem. Commun.*, 2012, **48**, 3321–3323.
8 K. C. Hewitt, L. Y. Beaulieu and J. R. Dahn, *J. Electrochem. Soc.*, 2001, **148**, A402–A410.
9 J. Li, A. Smith, R. J. Sanderson, T. D. Hatchard, R. A. Dunlap and J. R. Dahn, *J. Electrochem. Soc.*, 2009, **156**, A283–A288.
10 L. Baggetto, J. C. Jumas, H. T. J. M. Hintzen and P. H. L. Notten, *Electrochim. Acta*, 2010, **55**, 6617–6631.
11 L. Baggetto, N. J. Dudney and G. M. Veith, *Electrochim. Acta*, 2013, **90**, 135–147.
12 G. Kresse and J. Furthmuller, *Phys. Rev. B: Condens. Matter*, 1996, **54**, 11169–11186.
13 G. Kresse and D. Joubert, *Phys. Rev. B: Condens. Matter Mater. Phys.*, 1999, **59**, 1758–1775.
14 P. E. Blochl, *Phys. Rev. B: Condens. Matter*, 1994, **50**, 17953–17979.
15 I. A. Courtney, J. S. Tse, O. Mao, J. Hafner and J. R. Dahn, *Phys. Rev. B: Condens. Matter*, 1998, **58**, 15583–15588.
16 G. Henkelman, B. P. Uberuaga and H. Jónsson, *J. Chem. Phys.*, 2000, **113**, 9901–9904.
17 D. Larcher, D. Bonnin, R. Cortes, I. Rivals, L. Personnaz and J.-M. Tarascon, *J. Electrochem. Soc.*, 2003, **150**, A1643–A1650.
18 A. Darwiche, M. T. Sougrati, B. Fraisse, L. Stievano and L. Monconduit, *Electrochem. Commun.*, 2013, **32**, 18–21.
19 C. J. Wen, B. A. Boukamp, R. A. Huggins and W. Weppner, *J. Electrochem. Soc.*, 1979, **126**, 2258–2266.
20 A. Patterson, *Phys. Rev.*, 1939, **56**, 978–982.
21 K. Edström, T. Gustafsson and J. O. Thomas, *Electrochim. Acta*, 2004, **50**, 397–403.
22 P. C. Kemeny, J. G. Jenkin, J. Liesegang and R. C. G. Leckey, *Phys. Rev. B: Solid State*, 1974, **9**, 5307–5315.
23 Y.-M. Kim, J. He, M. D. Biegalski, H. Ambaye, V. Lauter, H. M. Christen, S. T. Pantelides, S. J. Pennycook, S. V. Kalinin and A. Y. Borisevich, *Nat. Mater.*, 2012, **11**, 888–893.

